Reconstruction techniques in angular correlation of positron annihilation experiments

1989 J. Phys.: Condens. Matter 1 SA1

(http://iopscience.iop.org/0953-8984/1/SA/001)

J. Phys.: Condens. Matter **1** (1989) SA1–SA16. Printed in the UK

Reconstruction techniques in angular correlation of positron annihilation experiments

Louis M Pecora
Code 6341, Naval Research Laboratory, Washington DC 20375, USA

Received 12 December 1988

Abstract. Various techniques for the reconstruction of momentum densities from 2D-ACPAR and 1D-ACPAR (angular correlation of positron annihilation radiation) data are reviewed. Emphasis is placed on spherical harmonic reconstruction techniques. Results of the reconstruction of the Fermi surface of vanadium are included. The possibility of obtaining wavefunction or quantum density matrix information from the momentum density is also mentioned.

1. Why reconstruction?

Angular correlation of positron annihilation (ACPAR) experiments measure a distribution which is close to the momentum density of a solid, $\rho(\boldsymbol{p})$, but they do not measure $\rho(\boldsymbol{p})$ directly. Rather they measure an integral of $\rho(\boldsymbol{p})$ over a straight line (two-dimensional ACPAR) or flat plane (one-dimensional ACPAR) in momentum space. Figure 1 shows a typical situation in two-dimensional ACPAR (hereafter referred to as 2D-ACPAR). In this sense, the data are a 'projection' of $\rho(\boldsymbol{p})$ onto a lower-dimensional space.

In addition, electronic many-body effects require that a different distribution, $\rho^{2\gamma}(\boldsymbol{p})$, be used in place of $\rho(\boldsymbol{p})$ in the formulation of the relationship between the data and the momentum density. For the purposes of this article this difference will be ignored and $\rho(\boldsymbol{p})$ will be written, even though $\rho^{2\gamma}(\boldsymbol{p})$ is required.

The data will be defined by the resolved electron momenta, p_z in 1D-ACPAR and p_x and p_y in 2D-ACPAR. The sample orientation will also determine the nature of the data. The orientation is given by a rotation, R, from the laboratory frame of reference to a fixed frame in the sample (usually aligning with the crystallographic axes). These dependences are explicitly shown in all the equations by writing $n^R(p_z)$ for 1D-ACPAR and $n^R(p_x, p_y)$ for 2D-ACPAR.

The relationships between $\rho(\boldsymbol{p})$ and the data are

$$\text{data} = n^R(p_z) = \int\int_{-\infty}^{+\infty} \rho(\boldsymbol{p})\, \mathrm{d}p_x\, \mathrm{d}p_y \tag{1}$$

$$\text{data} = n^R(p_x, p_y) = \int_{-\infty}^{+\infty} \rho(\boldsymbol{p})\, \mathrm{d}p_z \tag{2}$$

for 1D- and 2D-ACPAR, respectively.

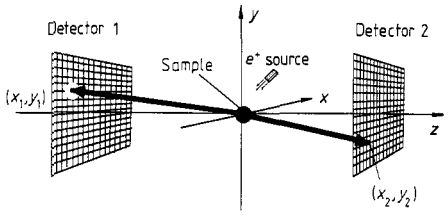

Figure 1. Typical 2D-ACPAR arrangement. The equations relating the positions of the detected gamma rays to the resolved momenta are $x_1 + x_2 = \Delta x \sim p_x$, $y_1 + y_2 = \Delta y \sim p_y$; in Fourier-space $p_x\, m_e c = \theta_x$, $p_y/m_e c = \theta_y$ (mrad).

Because of the intimate relationship between $\rho(\boldsymbol{p})$ and the electronic wavefunction, it would be especially convenient to be able to extract $\rho(\boldsymbol{p})$ from the data. The process of reconstruction is an attempt to do just this. Several reconstruction techniques have been applied over the last two decades to ACPAR data. Before reviewing these individual techniques some mathematical ideas need to be explored.

2. The mathematics of the reconstruction problem

The problem of obtaining a function from its integrals over planes or lines was first solved by Radon (1917). In practice, applications of any reconstruction technique, except in some simple situations, require a computer. Thus, it is only in the last two decades that reconstruction solutions have proliferated and have been successfully applied in many fields. For a good mathematical overview of the reconstruction problem the reader is referred to Deans (1983).

One of the most useful mathematical results in developing reconstruction techniques and algorithms is the central slice theorem (Deans 1983). There are 1D-ACPAR and 2D-ACPAR versions of this theorem. The two-dimensional version is as follows: the Fourier transform of the data equals the Fourier transform of $\rho(\boldsymbol{p})$ restricted to a plane in Fourier space whose normal is given by the rotation R. This is illustrated in figure 2. The one-dimensional version has the Fourier transform of the data being equal to the Fourier transform $\rho(\boldsymbol{p})$ restricted to a *line* in Fourier space the orientation of which is given by the rotation R.

Mathematically, if $\sigma(\boldsymbol{r})$ is the Fourier transform of $\rho(\boldsymbol{p})$ and if FT stands for Fourier transform (with respect to all resolved momenta variables in the data)

$$\mathrm{FT}[n^R(p_z)] = \sigma(\boldsymbol{r})|_{z=0} \tag{3}$$

$$\mathrm{FT}[n^R(p_x, p_y)] = \sigma(\boldsymbol{r})|_{x=0,y-0} \tag{4}$$

for 1D- and 2D-ACPAR, respectively, where x, y, and z are the coordinates in the rotated system. These relations are easy to derive from equations (1) or (2) by writing equations (1) or (2) as Fourier transforms in which the Fourier variable(s) conjugate to the integral momenta variables are constrained to be zero. Relations (3) and (4) immediately suggest schemes to reconstruct $\rho(\boldsymbol{p})$ from the data by going to Fourier space. Several have been applied to ACPAR data and are reviewed below.

Not all reconstruction techniques need to involve Fourier transforms. Several have been developed which involve analysis and algorithms in momentum space only. These are also reviewed below.

Three major categories of reconstruction schemes are covered here. The first is back-projection techniques which are commonly used in medical applications, like CAT scans.

The second is a restricted problem of reconstructing $\rho(\boldsymbol{p})$ on a plane in momentum space. The third uses an expansion of $\rho(\boldsymbol{p})$ in spherical harmonics.

One further problem actually remains. Although reconstructions can be done with any of these schemes on almost any available data, the quality of the reconstruction is not always immediately apparent. In other words, how much reliance should one place on the reconstruction? With few exceptions this remains a largely unaddressed problem. Yet this problem remains central to the question of reconstruction.

One approach, used in many other data analysis schemes, is to calculate the expected error based on the assumption of statistically independent error distributions for each data point. This leads to the calculation of the deviation or mean square error $\Delta\rho^2(\boldsymbol{p})$ at each point in momentum space. For example, for 2D-ACPAR if the reconstruction scheme, whatever it may be, is written as a (linear) operator $\mathcal{R}(\boldsymbol{p}; R, p_x, p_y)$, then the mean square error is given by

$$\Delta\rho^2(\boldsymbol{p}) = [\mathcal{R}(\boldsymbol{p}; R, p_x, p_y)]^2 \Delta n^2(R, p_x, p_y) \tag{5}$$

where $\Delta n^2(R, p_x, p_y)$ is the mean square error for the R sample orientation at the resolved momenta p_x, p_y and all integrations and sums over repeated variables are implicit on the right-hand side of equation (5). The calculation of $\mathcal{R}(\boldsymbol{p}; R, p_x, p_y)$ is itself a formidable task, so the calculation of $[\mathcal{R}(\boldsymbol{p}; R, p_x, p_y)]^2$ can be quite complicated and time consuming. Nevertheless, it remains important for all reconstruction schemes. As yet, it also appears to remain unsolved or not performed for any reconstruction scheme. It is the next important problem to solve in this type of analysis of positron annihilation data.

If equation (5) cannot be used, then there are other approaches to estimating the error in a reconstructed image. These include the reconstruction of noise (representing errors in the data), the reconstruction of models and, better still, theoretical momentum densities. The reader is referred to Mijnarends (1967, 1979), Pecora (1987), and Hansen (1980) for more on this important topic.

2.1. Backprojection reconstruction

The basic idea here is to use the central slice theorem to get an estimate $\sigma'(\boldsymbol{r})$ of $\sigma(\boldsymbol{r})$ in the hope that in some sense $\sigma'(\boldsymbol{r}) \simeq \sigma(\boldsymbol{r})$. Then using the inverse Fourier transform, $\rho'(\boldsymbol{p})$ can be reconstructed with the hope that $\rho'(\boldsymbol{p}) \simeq \rho(\boldsymbol{p})$. The calculation of $\sigma(\boldsymbol{r})$ from the data involves taking the Fourier transform of the data and then interpolating in Fourier space to get $\sigma(\boldsymbol{r})$ at points not in the planes defined by the central slice theorem.

Most 2D-ACPAR versions of this technique are developed for reconstruction of $\rho(\boldsymbol{p})$ in a plane in momentum space. The whole three-dimensional object, $\rho(\boldsymbol{p})$, is then built up from laminating many planes together. This requires sets of data that are taken by rotating the sample about one axis only, that is all the Rs are rotations of various magnitudes about the same axis. This greatly restricts the acquisition of data, but in high-symmetry situations a choice of one of the high-symmetry axes as the rotation axis can facilitate the process.

The calculations in Fourier space can actually be done analytically if a suitable 'cut-off' is chosen (Deans 1983, Brooks and DiChiro 1976, Cormack 1973). One is then left with a scheme in which, with a modifying filter, the data sets (or profiles) are translated over a line which goes through the origin at an angle equal to the orientation of the sample with respect to that plane and are added together over the same plane in

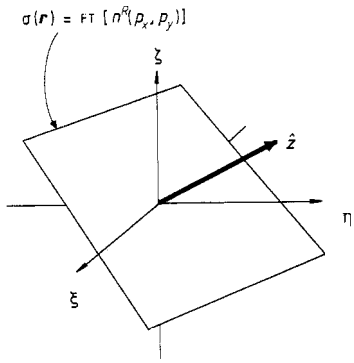

Figure 2. Central slice theorem for 2D-ACPAR in Fourier space.

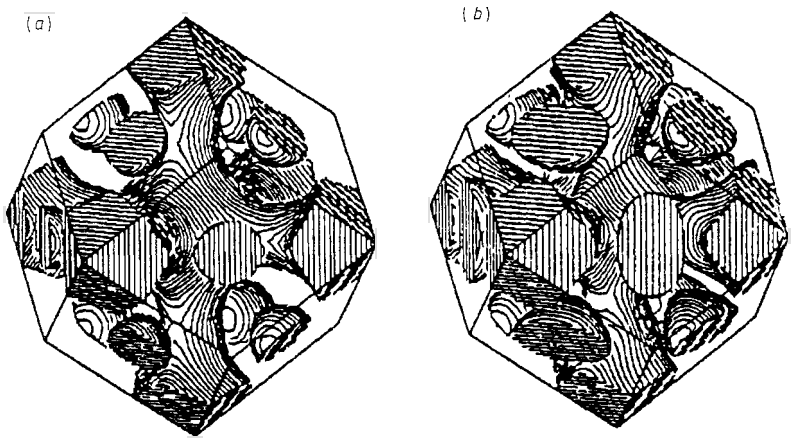

Figure 3. Reconstruction of the third zone Fermi surface of vanadium by Manuel (1982): (*a*) experiment, (*b*) theory.

momentum space. This view of the reconstruction process is the origin of the term 'back projection'.

The first use of back projection in the reconstruction of the momentum density from 2D-ACPAR was also the first fully three-dimensional reconstruction (Berko 1983). This reconstruction of the momentum density of Cu shows, correctly, many of the anisotropies in the $\rho(\boldsymbol{p})$ of Cu. There was also a later attempt by this group (Sinclair *et al* 1982) to extract many-body enhancement parameters from the reconstruction.

Another back-projection reconstruction was done by Waspe and West (1982) on 2D-ACPAR from Gd. Analysis of the $\rho(\boldsymbol{p})$ of Gd was aided in this work by the additional folding of the Gd $\rho(\boldsymbol{p})$ back into the first Brillouin zone using the Lock–Crisp–West (LCW) theorem (Lock *et al* 1972) to show the Fermi surface outlines.

A more recent use of the LCW theorem in conjunction with back-projection reconstruction was by Manuel (1982) in the reconstruction of the third-zone Fermi surface of vanadium. As can be seen in figure 3, this yielded a reconstruction which was in very good agreement with band-structure predictions. However, it proved difficult to get the second-zone Fermi surface. This difficulty was overcome with the use of the spherical-harmonic Fourier-space reconstruction scheme reviewed in §§ 2.3.2 and 2.3.4.

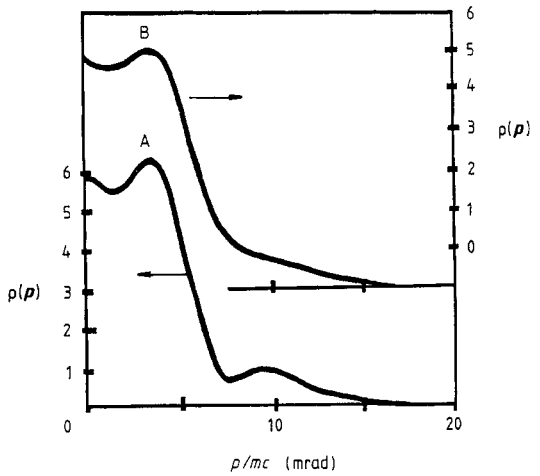

Figure 4. Reconstruction of $\rho(\boldsymbol{p})$ for Cu (curve A) and $Cu_{92}Ge_8$ (curve B) along [100] showing the changes in the 5–9 mrad region (Pecora and Ehrlich 1981).

Recently, Suzuki and Tanigawa (1988) have implemented a Fourier-space reconstruction scheme based on the central slice theorem which does not use the analytically calculated back-projection filter, but directly interpolates in Fourier space to get $\sigma(\boldsymbol{r})$ and then calculates the inverse Fourier transform to get $\rho(\boldsymbol{p})$. Whether this is superior to other methods or, perhaps, more appropriate in certain circumstances remains to be seen. At present their model calculations require four to six data directions for high-quality reconstructions.

2.2. *Planar* 2D *reconstruction*

In certain experimental cases, often called point geometry set-ups, one gets data which is 2D-ACPAR, but restricted to a particular plane in momentum space. In this case the original formulation of Cormack (1963, 1964) or a variation of it can be used to reconstruct $\rho(\boldsymbol{p})$ in the momentum space plane.

Mathematically the problem is one of obtaining data whose relation to $\rho(\boldsymbol{p})$ is

$$n^R(p_x, p_y) = \int_{-\infty}^{\infty} \rho(\boldsymbol{p})\, \mathrm{d}p_z \tag{6}$$

with p_x fixed. It has been shown by Pecora and Ehrlich (1979) that $\rho(\boldsymbol{p})$ can be reconstructed from the restricted data in equation (6) using a scheme similar to that of Cormack (1963, 1964). This expands $\rho(\boldsymbol{p})$ and the data in a polar Fourier series and the reconstruction is done by the resulting relationships between the series' coefficients, namely

$$\rho(\boldsymbol{p}) = \sum_m \rho_m \, \mathrm{e}^{\mathrm{i}m\theta} \tag{7}$$

$$n^R(p_x, p_y) = \sum_m n_m(p) \, \mathrm{e}^{\mathrm{i}m\theta}. \tag{8}$$

This scheme was applied to the reconstruction of $\rho(\boldsymbol{p})$ in the (011) and (111) planes of Cu and α-phase $Cu_{1-x}Ge_x$ alloys for $x = 0.03$, 0.06, and 0.08 (Pecora and Ehrlich 1985). Figure 4 shows the results of this reconstruction in Cu and $Cu_{92}Ge_8$ along the [100] direction. The difference in the anisotropy in the 6–8 mrad region is obvious and was

attributed to changes in the s–d hybridisation in the α-phase of these alloys as Ge is added to Cu (Pecora and Ehrlich 1981).

Other work using planar 2D reconstruction by Kortrym-Sznajd (1982) has shown that many variations on this approach can lead to workable reconstruction schemes. Formulae like equations (7) and (8) can also be used to reconstruct three-dimensional images of $\rho(\boldsymbol{p})$ from 2D-ACPAR similar to the back-projection approach of laminating the planar reconstructions together. This appears not to have been attempted, as yet.

2.3. *Spherical harmonic reconstruction*

Many reconstruction schemes have as their basis the expansion of the desired object, $\rho(\boldsymbol{p})$, in certain functions along with a technique for extracting the unknown expansion coefficients from the data. The use of spherical harmonic expansions has been a prominent, as well as fruitful, approach in positron annihilation reconstruction schemes. Spherical harmonic reconstruction (SHR) schemes have been applied to 1D-ACPAR and 2D-ACPAR both directly in momentum space and through Fourier space. The developments of these schemes are interrelated.

2.3.1. 1D-ACPAR momentum space spherical harmonic reconstruction. The first reconstruction scheme for the extraction of $\rho(\boldsymbol{p})$ from the experimental data was devised by Mijnarends (1967) using a SHR method in momentum space. The basis of this approach is to write

$$\rho(\boldsymbol{p}) = \sum_{lm} \rho_{lm}(p) Y_{lm}(\theta_p, \varphi_p) \tag{9}$$

where p, θ_p, and φ_p are the spherical coordinates of p and Y_{lm} are the spherical harmonics.

Mijnarends then showed that one can expand the data in a similar way:

$$n^R(p_z) = \sum_{lm} n_{lm}(p_z) Y_{lm}(\beta, \alpha). \tag{10}$$

where β, α define the sample orientation.

This leads to the relationship between expansion coefficients which allows reconstruction, namely

$$\rho_{lm}(p) = \int_0^p \frac{\mathrm{d}^2 n_{lm}(p_z)}{\mathrm{d}p_z^2} P_l(p_z/p)\, \mathrm{d}p_z. \tag{11}$$

where the P_l are Legendre polynomials.

Mijnarends applied this to Cu 1D-ACPAR data (Mijnarends 1969) to show that using this technique one could reveal structure in $\rho(\boldsymbol{p})$ which was not obvious from the data. For example the anisotropy in $\rho(\boldsymbol{p})$ from 6–8 mrad comparing the two directions [100] and [110] stands out and was later shown to be intimately connected with the band structure (Mijnarends 1972).

One restriction on the above spherical harmonic expansion is that the number of terms in each reconstruction must be less than or, at most, equal to the number of independent data sets available. This restriction has some consequence in positron annihilation since obtaining large data sets has been difficult and time consuming. The result of attempting reconstruction with a small number of data sets can be seen in the wildly oscillating results for Cu, Ag, Au, Mg, and Cd (Pajak *et al* 1976) and the featureless

momentum density reconstructed from three Compton profile directions (Das *et al* 1988), although the latter also suffers from poor data resolution.

2.3.2. 1D-ACPAR Fourier-space spherical harmonic reconstruction. A method similar to Mijnarends momentum space scheme was devised by Hansen (1980). This uses the central slice theorem to obtain $\sigma(\boldsymbol{r})$ on lines in Fourier space. The next step is to expand $\sigma(\boldsymbol{r})$ in a series of spherical harmonics

$$\sigma(\boldsymbol{r}) = \sum_{lm} \sigma_{lm}(r) Y_{lm}(\theta, \varphi) \tag{12}$$

where p, θ, and φ are again the spherical coordinates of $\boldsymbol{r}$. It is easily (Deans 1983) shown that the coefficients $\sigma_{lm}(r)$ are related to the coefficients $\rho_{lm}(p)$ of the expansion of $\rho(\boldsymbol{p})$ in spherical harmonics by a Hankel transform

$$\rho_{lm}(p) \simeq \int_0^\infty j_l(pr)\sigma_{lm}(r)r^2 \, \mathrm{d}r \tag{13}$$

where $j_l(\mathrm{pr})$ is a spherical Bessel function of the first kind. Thus, like Mijnarend's (1967) 1D-ACPAR momentum space SHR, the scheme of Hansen *et al* (1987) gives a similar expansion of $\rho(\boldsymbol{p})$, and is likewise limited to the same restriction that the number of coefficients $\rho_{lm}(p)$ determined is less than or equal to the number of independent data sets.

This technique was applied to silicon. Hansen *et al* (1987) were able to extract the anisotropic contribution to $\rho(\boldsymbol{p})$ in silicon by this method. In the same paper they make attempts to obtain error estimates on their reconstructions, something that is often sadly lacking in other reconstruction work.

2.3.3. 2D-ACPAR momentum space spherical harmonic reconstruction. Majumdar (1971) showed, using elegant mathematical analysis, that it was possible to reconstruct $\rho(\boldsymbol{p})$ from 2D-ACPAR data using a spherical harmonic expansion. The reconstruction was done in momentum space and, in a sense, is a higher dimensional version of Mijnarend's scheme.

The first step in this analysis is to rewrite equation (9) in a rotated coordinate system, taken to be that of the laboratory frame

$$\rho(\boldsymbol{p}) = \sum_{lmm'} D^l_{mm'}(R)\rho_{lm}(p)Y_{lm'}(\theta'_p, \varphi'_p) \tag{14}$$

where $D'_{mm'}(R)$ is the matrix of coefficients relating spherical harmonics in the sample frame to those in the laboratory frame and θ'_p and φ'_p are spherical coordinates of $\boldsymbol{p}$ in the laboratory frame. He then showed that the data for each data set could be expanded in polar coordinates, s and φ'_p, in the data plane

$$n^R(p_x, p_y) = \sum_{lmm'} D^l_{mm'}(R)g_{lm'}(s)\, \mathrm{e}^{\mathrm{i}m'\varphi'_p}. \tag{15}$$

This means that the polar Fourier coefficients $g_{lm}(s)$ can in principle be found from one data set. He then showed that a Mellin transform relates $\rho_{lm}(p)$ and $g_{lm}(s)$. This transform is a complicated contour integral in complex variables involving hypergeometric functions. However, the important thing to note is that one data set provides information on many $\rho_{lm}(p)$ coefficients. This is in contrast to the 1D-ACPAR SHR schemes and it results from the two-dimension nature of the data. With this approach one can get more $\rho_{lm}(p)$ than there are data sets.

Table 1. Comparison between high- and low-symmetry cases in 2D-ACPAR reconstruction using double-precision computer calculations.

Number of data sets	*R* Euler angles (deg) α	β	γ	Number of coefficients	Highest l-value
1 (high symmetry)	0	0	0	1	0
1 (low symmetry)	71	33	0	10	16
2 (high symmetry)	0	0	0	—	—
	0	45	0	5	10
2 (low symmetry)	71	33	0	—	—
	54	43	0	30	32

Table 2. The four basic types of reconstruction technique using spherical harmonics (SHR), listing their authors

Correlation method	SHR technique: Momentum space	Fourier space
1D-ACPAR	Mijnarends (1967)	Hansen (1980)
2D-ACPAR	Majumdar (1971) (Howells and Osmon 1972)	Pecora (1987)

On a practical level, one would want to use more than one data set, since information on particular $\rho_{lm}(p)$ coefficients may not be present or may be less than the noise or error level. This can occur, for example, in data planes that are also high-symmetry planes in the sample, so that the spherical harmonics have nodes, or zeros, in these planes and therefore do not contribute to the data.

Because of the complexity involved, Majumdar's (1971) technique was apparently never applied to 2D-ACPAR data. However, it stimulated the development of another similar scheme which turned out to be practical and at the same time enjoyed the advantage of having, in principle, no restriction on the number of coefficients of $\rho(\boldsymbol{p})$ determined from the data.

Howells and Osmon (1972) also developed a reconstruction scheme similar to that of Majumdar (1971). This include the expansion of the coefficients in special functions depending on the radial variable r. Apparently, this method has never been tried on data.

2.3.4. 2D-ACPAR Fourier-space spherical harmonic reconstruction. This technique was developed by Pecora (1987) and in its relationship to Majumdar's (1971) 2D-ACPAR SHR scheme is analogous to that of Hansen (1980) and its relationship to Mijnarend's (1967) scheme for 1D-ACPAR data. This two-dimensional scheme was also developed independently by Vogel *et al* (1986) who applied it successfully to image reconstruction electron microscopy scans. They also show an extention to this method which expands the coefficients of $\rho(\boldsymbol{p})$ in special functions. This last extension will not be discussed here.

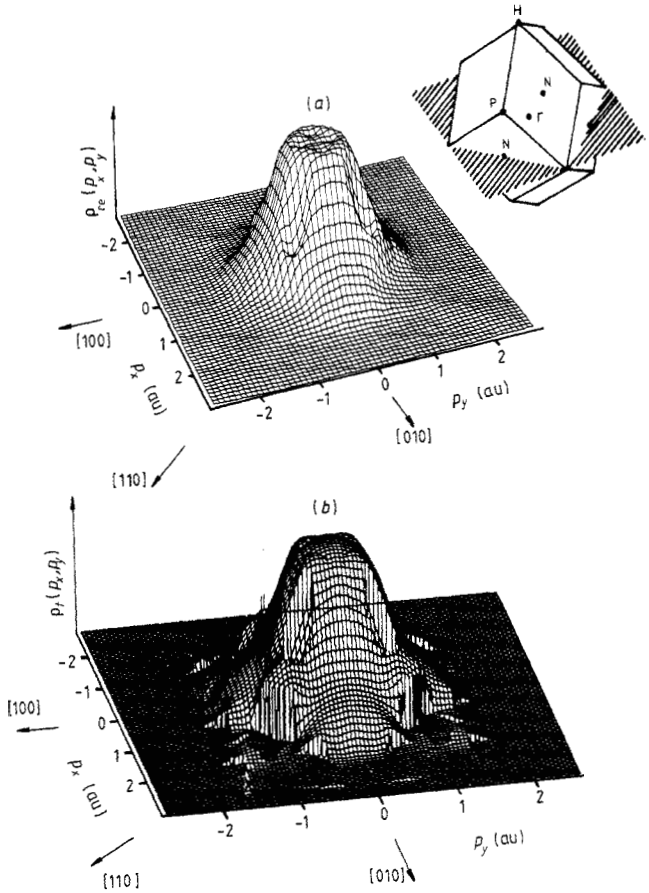

Figure 5. Vanadium $\rho(\boldsymbol{p})$ in the (001) plane: (*a*) reconstructed data from experiment, and (*b*) theory (Pecora *et al* 1988).

Following Majumdar (1971) we expand $\rho(\boldsymbol{p})$ in a series of spherical harmonics. As in Hansen's work, this leads to a series expansion of $\sigma(\boldsymbol{r})$ in spherical harmonics. Now, we rotate to a coordinate system in Fourier space that is aligned with the laboratory coordinate system. This gives for $\sigma(\boldsymbol{r})$

$$\sigma(\boldsymbol{r}) = \sum_{lmm'} D^{l}_{mm'}(R)\sigma_{lm}(r)Y_{lm'}(\theta', \varphi'). \tag{16}$$

Because $Y_{lm}(\theta, \varphi) = N_{lm}P_{lm}(\cos\theta)\,e^{im\varphi}$, it is natural to take the polar Fourier transform of $\sigma(\boldsymbol{r})$. Using equation (16) this gives

$$\sigma^{R}_{m'}(r) = \sum_{lm} D^{l}_{mm'}(R)\sigma_{lm}(r)P_{lm'}(\cos\theta')\,N_{lm'} \tag{17}$$

which holds for $m' = 0, 1, 2, \ldots$. This means that, as in Majumdar's (1971) momentum space scheme, we can find several unknown coefficients $\sigma_{lm}(r)$ from one data set. Since $\rho_{lm}(p)$ and $\sigma_{lm}(r)$ are related through a Hankel transform (equation (13)) we would get many terms in the expansion of $\rho(\boldsymbol{p})$. Again, we would want numerical stability when

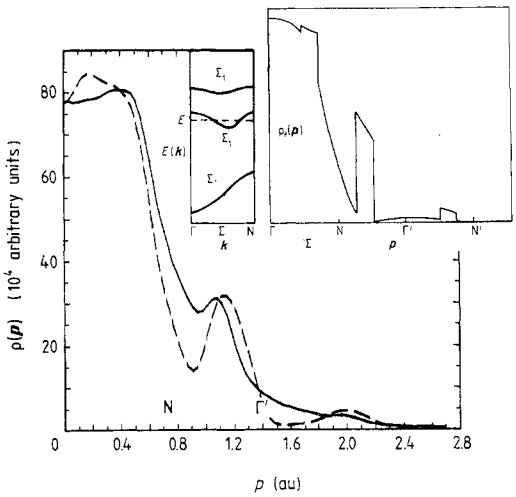

Figure 6. Radial slice of $\rho(\boldsymbol{p})$ in figure 5 along the [110] direction: ——, reconstructed experiment; – – –, reconstructed theory. Inset: pure theory, $\rho_t(\boldsymbol{p})$ (Pecora *et al* 1988).

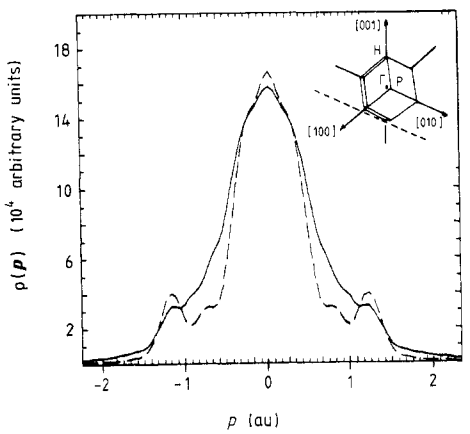

Figure 7. Radial slice of $\rho(\boldsymbol{p})$ in figure 5 along a direction parallel to [010] in the (001) plane and displaced 1.34 au from the origin: ——, reconstructed experiment; – – –, reconstructed theory. Inset: direction of slice with respect to crystallographic axes.

solving equation (17), so we would actually want to have several data sets. But we would get more coefficients $\rho_{lm}(p)$ than we had data sets, in contrast to the 1D-ACPAR case.

In the case of crystal symmetry one gets even better reconstructions by using the appropriate symmetry lattice harmonics in place of the spherical harmonics. These are linear combinations of spherical harmoncis. This is one of the advantages of using lattice harmonics. The spherical harmonics which are not appropriate are automatically omitted and the resulting reconstruction has the proper symmetry. This is implemented below for cubic harmonics.

Another feature in the 2D-ACPAR reconstruction work stands out more clearly here than elsewhere and that is that data sets are best taken not in high-symmetry planes, as is traditionally done in positron annihilation, but in low-symmetry planes. This is true for many kinds of reconstruction schemes, but becomes more apparent here when one examines the inversion of equation (17) to obtain $\sigma_{lm}(r)$. If the data is taken in high-symmetry planes, then the problem of some of the spherical harmonics having nodes in that plane prevents solution of equation (17) for any arbitrary number of terms. Table 1 shows a comparison between high- and low-symmetry cases when using double-

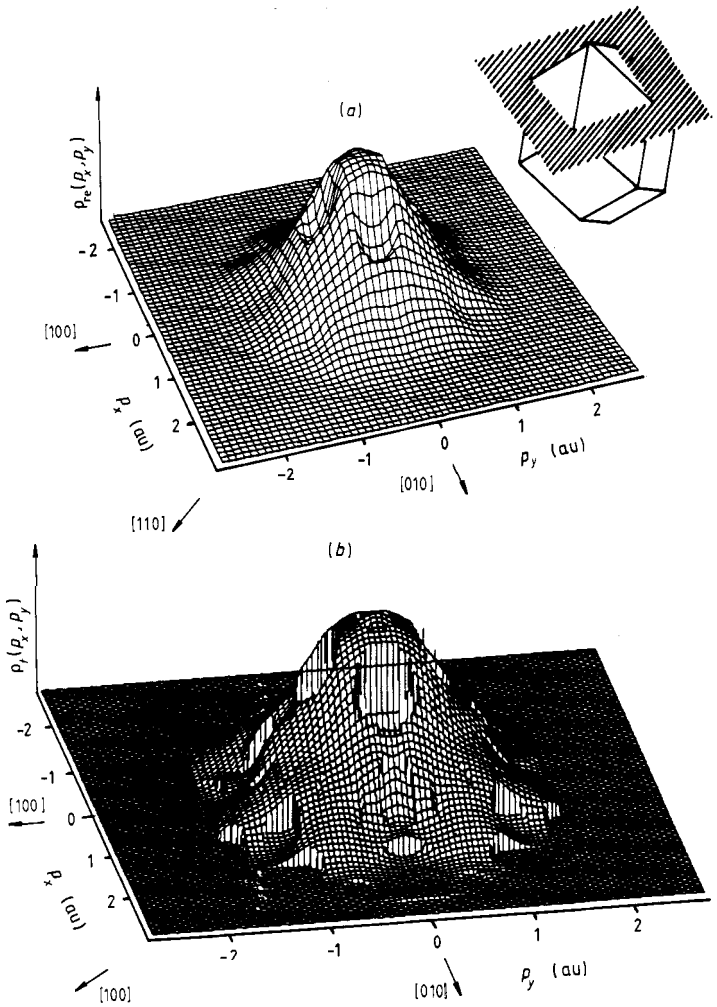

Figure 8. A surface of $\rho(\boldsymbol{p})$ parallel to the (001) plane displaced 4.14 mrad (π/a) from the origin along the [001] axis (*a*) reconstructed experiment, (*b*) theory (Pecora *et al* 1988).

precision (8 byte floating-point) computer calculations. Hence, for two directions in cubic symmetry, one can get the first 30 coefficients in the expansion of $\rho(\boldsymbol{p})$. Of course, we have not done an error analysis of this case. This has been done elsewhere (Pecora 1987) for this situation.

With the implementation of a 2D-ACPAR Fourier-space SHR scheme, the four basic types of reconstruction using spherical harmonics are now available. The relationship between these is evident from table 2, which lists the authors of the main techniques in the field of positron annihilation and Compton scattering.

3. Reconstruction of the momentum density of vanadium

The 2D-ACPAR Fourier-space SHR scheme was applied to four data sets taken in the (100), (110), (111) and (211) planes of vanadium. The details of the experiment are given

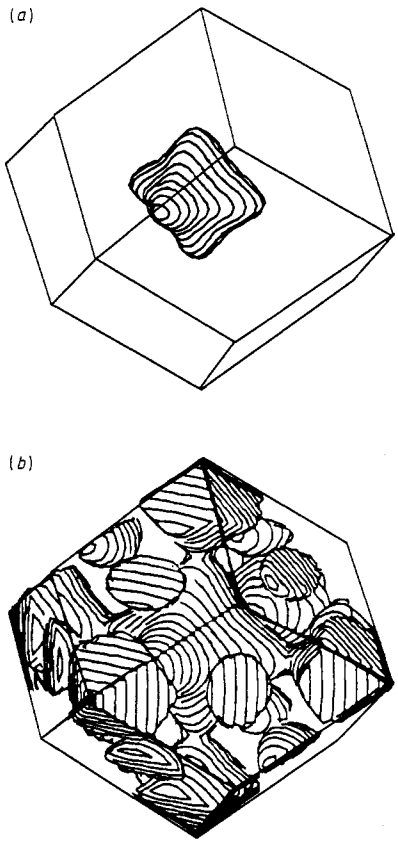

Figure 9. Reconstructions of (*a*) the second and (*b*) third zone Fermi surfaces of vanadium.

elsewhere (Bisson *et al* 1982). The details of this reconstruction are given in Pecora *et al* (1988). The resolution of the data was 0.041×0.068 au^2 and the total number of counts was approximately 6×10^7 for each data set. The largest number of cubic harmonic terms obtainable in the reconstruction under these circumstances was 40. However, only the first 25 were of a large enough amplitude to affect the reconstruction. The remaining 26–40 were below the expected noise level and their addition did not affect the results.

These results were compared to theory (Singh and Singru 1982), both directly and by reconstruction of the theoretical $\rho(\boldsymbol{p})$ from 'data' generated by the theory in the same planes as in the experiment.

Figure 5 shows the results of the reconstruction for the (001) plane of vanadium. In the same figure the theoretical $\rho(\boldsymbol{p})$ in the same plane is shown for comparison. As would be expected, the theory shows sharper structure, but the main features of the theory are present in the reconstruction. The depressions caused by the N-centre ellipsoids (NCE) along the ⟨110⟩ directions are clearly visible. The depressions caused by the Γ-centred octahedral (GCO) hole-bands and, to a lesser extent, the jungle gym arms (JGA) are evident further out in the same directions.

Two 'cuts' through the surfaces in figure 5 are shown in figures 6 and 7. In figure 6 are radial slices along [110], one from the 2D-ACPAR reconstruction and the other from reconstructed theoretical data. There is excellent agreement between the two and a lack

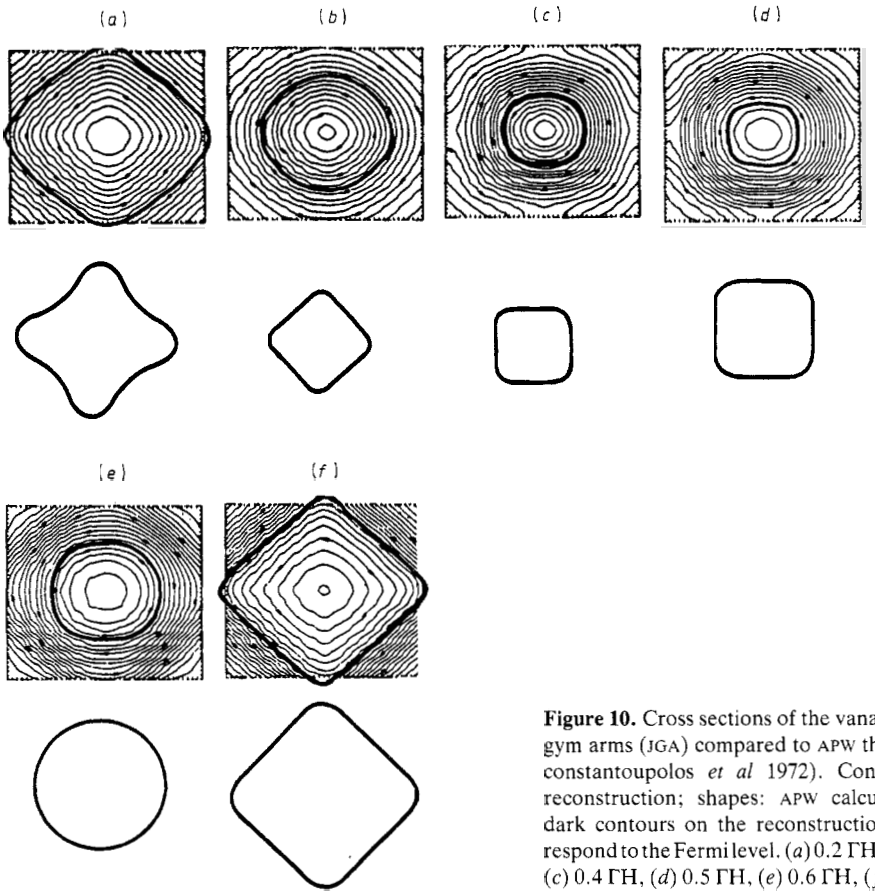

Figure 10. Cross sections of the vanadium jungle gym arms (JGA) compared to APW theory (Papaconstantoupolos *et al* 1972). Contours plots: reconstruction; shapes: APW calculation. The dark contours on the reconstruction plots correspond to the Fermi level. (*a*) 0.2 ΓH, (*b*) 0.3 ΓH, (*c*) 0.4 ΓH, (*d*) 0.5 ΓH, (*e*) 0.6 ΓH, (*f*) 0.7 ΓH.

of artifacts in the theoretical reconstruction. In figure 7 the slices are tangent to a circle of radius 1.34 au. This figure shows not only a good agreement between the reconstructed theory and experiment, but also displays good resolution, which is essentially angular resolution.

Figure 8 shows a comparison of {001} surfaces of the theory (without reconstruction) and the reconstructed experimental data. The surfaces in this figure are displaced 4.14 mrad from the origin along the [001] axis.

Since one has $\rho(\boldsymbol{p})$ it is posible to follow the method of Lock *et al* (1972) and calculate an approximation to the number density in $\boldsymbol{k}$-space, $\nu(\boldsymbol{k})$, and, therefore, plot the Fermi surfaces of the material. Knowing $\nu(\boldsymbol{k})$ in this way does not give the true number density, since the positron selectively annihilates with the electrons. This means that in order to choose values of ν (say ν_2 and ν_3) to correspond to Fermi levels of the second and third zones we need another criterion. In this case the criterion for the third zone was to choose ν_3 so as to keep the size of the NCEs equal to the values found by Parker and Halloran (1974). For the second zone the only criterion was to keep it near the size found by the band theory. Nothing quantitative is done with the second zone surface.

Figure 9 shows a reconstruction of the second and third zone Fermi surfaces. The agreement with theory (Singh and Singru 1982) and with previous work on a reconstructed vanadium Fermi surface (Manuel 1982) is very good. In addition this recon-

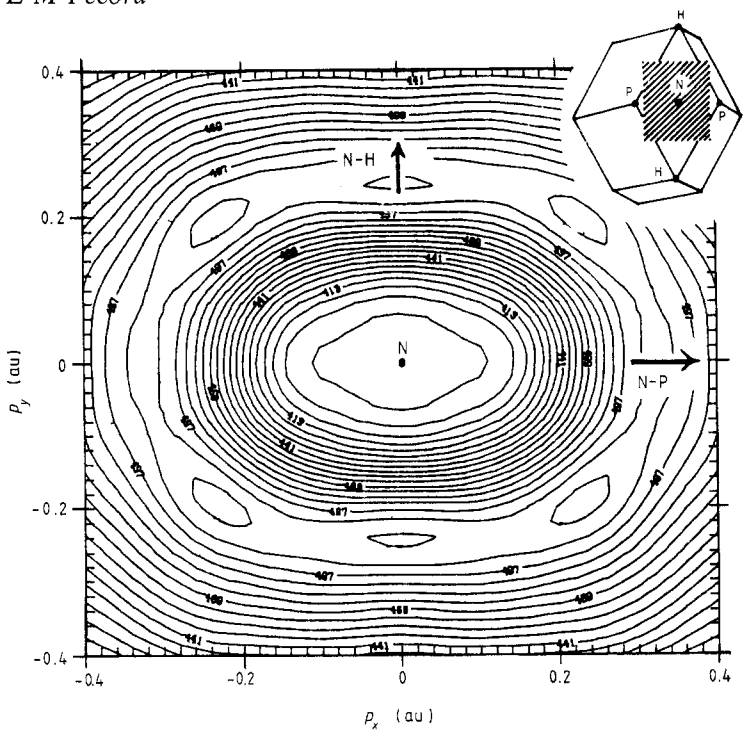

Figure 11. Cross section of the N-centred ellipsoids (Pecora *et al* 1988). Inset shows position and orientation of the cross section with respect to the crystal.

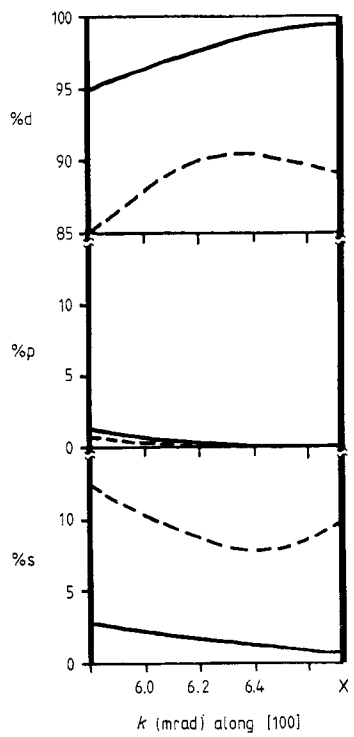

Figure 12. Percent s, p, and d contribution to the hybridised wavefunction from ≈5 to ≈9 mrad along [100] (Pecora 1986) of Cu (——) and $Cu_{92}Ge_8$ (– – –).

struction scheme has enabled the reconstruction of the second zone surface for the first time. Figure 10 shows cross sections of the JGA from the reconstruction compared to an APW calculation (Papaconstantopoulos *et al* 1972). The overall shape and size agree well. Figure 11 shows a cross section of the NCE. The ratio of the major to minor axes of the ellipses in this figure is 1.36, independent of what contour is chosen around the N point. This agrees well with the measurements of Parker and Halloran (1974) which was 1.27.

4. Reconstruction of the quantum density matrix

It is possible to take another step in the reconstruction process, namely to obtain information on the quantum density matrix of the bands contibuting to $\rho(\boldsymbol{p})$. The possibility of extracting quantum density matrices from experimental data has been under investigation for some time by many workers investigating x-ray scattering in solids (Goldberg and Massa 1983, Clinton and Massa 1972, Pecora 1986). A complete review of this topic is beyond the scope of this paper, but it is an appropriate area of investigation for anyone doing reconstruction of 2D-ACPAR data, since it might allow the possibility of obtaining information about wave functions from reconstructions. The reader is referred to Goldberg and Massa (1983), Clinton and Massa (1972) and Pecora (1986) for more thorough explanations, including the application of this technique to positron annihilation.

Any measurement α_q can be represented by the formula $\alpha_q = \mathrm{Tr}(\mathbf{P}O^q)$, where Tr is the trace operation, $\mathbf{P}$ is a population matrix (a quantum density matrix in a particular representation) and O^q is the operator corresponding to the measurement. For example in the case of positron annihilation, $\mathbf{P}$ is the population of the contributing bands and O^p would be the (selective) annihilation of the positron with those bands. Then $\rho(\boldsymbol{p}) = \mathrm{Tr}(\mathbf{P}O^p)$.

Pecora (1986) has shown that it is possible to use a constrained minimisation procedure to obtain $\mathbf{P}$ from $\rho(\boldsymbol{p})$. An application of this procedure to Cu and $Cu_{92}Ge_8$ is shown in figure 12. This demonstrates more quantitatively the suggestion that the s–d hybridisation was changing with Ge concentration (Pecora and Ehrlich 1981).

Because other one-particle observables exist, this implies that one can calculate other quantities (like the real-space charge density of only those electrons with certain $\boldsymbol{k}$-vectors) and compare them to other experiments and theory. The implications for positron annihilation are great, but much more work must be done on this topic to clarify the scheme and assure reliability of the quantum density matrix extracted.

References

Berko S 1983 *Positron Solid State Physics* ed. W Brandt and A Dupasquier (Amsterdam: North-Holland) p 118

Bisson P E, Descouts P, Dupanloup A, Manuel A A, Perreard E, Peter M and Sachot R 1982 *Helv. Phys. Acta* **55** 100

Brooks R A and DiChiro G 1976 *Phys. Med. Biol.* **21** 689

Clinton W L and Massa L J 1972 *Phys. Rev. Lett.* **29** 1363

Cormack A 1963 *J. Appl. Phys.* **34** 2722

—— 1964 *J. Appl. Phys.* **35** 2908

—— 1973 *Phys. Med. Biol.* **18** 195

Das G P, Bhagwat K V and Sahni V C 1988 *Phys. Rev.* A **36** 2984

Deans S R 1983 *The Radon Transform and Some of Its Applications* (New York: Wiley Interscience)

Goldberg M J and Massa L J 1983 *Int. J. Quantum Chem.* **24** 113
Hansen N K 1980 *HMI-Report* B **342**
Hansen N K, Pattison P and Schneider J R 1987 *Z. Phys.* B **66** 305
Howells M R and Osmon P E 1972 *J. Phys. F: Met. Phys.* **2** 277
Kortrym-Sznajd G 1982 *Positron Annihilation* ed. P G Coleman, S C Sharma and L M Diana (New York: North-Holland) p 346
—— 1988 *International Positron Workshop* unpublished
Lock D G, Crisp V H C and West R N 1972 *J. Phys. F: Met. Phys.* **3** 561
Majumdar C K 1971 *Phys. Rev.* B **4** 2111
Manuel A A 1982 *Phys. Rev. Lett.* **49** 1525
Mijnarends P E 1967 *Phys. Rev.* **160** 512
—— 1969 *Phys. Rev.* **178** 622
—— 1972 *Physica* **63** 235
—— 1979 *Positrons in Solids* ed. P Hautojärvi (Berlin: Springer)
Pajak J, Chabik St, Rozenfeld B and Kortrym-Sznajd G 1976 *Acta Phys. Pol.* A **50** 623
Papaconstantopoulos D, Anderson J R and McCaffrey J W 1972 *Phys. Rev.* B **5** 1214
Parker R D and Halloran M M 1974 *Phys. Rev.* B **9** 4130
Pecora L M 1986 *Phys. Rev.* B **33** 5987
—— 1987 *IEEE Trans. Nucl. Sci.* **NS-34** 642
Pecora L M and Ehrlich A C 1979 *Phys. Rev.* B **19** 719
—— 1981 *Phys. Rev. Lett.* **46** 1476
—— 1985 *Phys. Rev.* B **32** 708
Pecora L M, Ehrlich A C, Manuel A A, Singh A K, Peter M and Singru R M 1988 *Phys. Rev.* B **37** 6772
Pecora L M, Ehrlich A C, Manuel A A, Singh A K and Singru R M 1985 *Positron Annihilation* ed. P C Jain, R M Singru and K P Gopinathan (Singapore: World Scientific)
Radon J 1917 *Berichte Sachsische Akademie der Wissenshaften, Leipzig, Mathematisch-Physikalische Klasse 69* (Leipzig) p 262
Sinclair F, Farmer W S and Berko S 1982 *Positron Annihilation* ed. P G Coleman, S C Sharma and L M Diana (New York: North-Holland) p 322
Singh A K and Singru R M 1982 *J. Phys. F: Met. Phys.* **12** 685
Suzuki R and Tanigawa S 1988 *Proc. 8th Int. Conf. Positron Annihilation* unpublished
Vogel R H, Provencher S W, von Bonsdorff C-H, Adrian M and Dubochet J 1986 *Nature* **320** 533
Waspe R L and West R N 1982 *Positron Annihilation* ed. P G Coleman, S C Sharma and L M Diana (New York: North-Holland) p 328